5-2022

Layered Epoxide-Amine/Boron Nitride/Graphene Nanocomposites for Enhanced Multifunctional Shielding

Alyssa J. Necaise

Layered Epoxide-Amine/Boron Nitride/Graphene Nanocomposites for Enhanced Multifunctional Shielding

by

Alyssa J. Necaise

A Thesis
Submitted to the Honors College of
The University of Southern Mississippi
in Partial Fulfillment
of Honors Requirements

May 2022

Approved by:

Jeffrey Wiggins, Ph.D., Thesis Advisor,
School of Polymer Science and Engineering

Derek Patton, Ph.D., Director,
School of Polymer Science and Engineering

Sabine Heinhorst, Ph.D., Dean
Honors College

ABSTRACT

The development of high-power electromagnetic wave sources in the modern era has the ability to interfere with aircraft electronics and cause localized heating – necessitating advanced materials for electromagnetic interference (EMI) and thermal shielding. Multifunctional nanoparticles dispersed within polymer matrices can combat these issues; however, the best way to combine thermally and electrically conductive species to maximize electromagnetic interference shielding and thermal shielding is undetermined. Multifunctional layered epoxide/amine nanocomposites were prepared from tetra and octafunctional epoxide monomers (TGDDM and SU-8), 4,4-DDS tetrafunctional amine curative, and 1 wt.% hexagonal boron nitride nanoplatelets and/or 1 wt.% graphene nanoplatelets to form monolayer and bilayer films. Multilayer, vitrified nanocomposite laminates were prepared and characterized to quantify particle dispersion, layer orientation/integrity, rheological properties, and thermal properties via optical/scanning electron microscopy, FTMS rotational rheometry, thermogravimetric analysis, and laser flash diffusivity analysis. Monomer conversion throughout various cure profiles was quantified using ATR-FTIR spectroscopy. The data collected indicated that discrete layers were maintained throughout thermoset curing, with no hindrances in the rheological or thermal properties of the matrix. This suggests a new methodology for preparing layered, multifunctional EMI/thermal shielding materials with enhanced thermal conductivity.

Keywords: Electromagnetic interference shielding, Thermal shielding, Multifunctional nanoparticles, Epoxide/Amine

DEDICATION

I would like to dedicate this honors thesis first to God for everything I have been blessed to experience in my adventure of life, my mother for everything she has given me, and my family and friends who have supported me through four very challenging years of education. Finally, I want to recognize *Mr. Joel Myrick*, my high school polymer science career readiness instructor, for igniting my passion in polymer science by simply believing in me and entertaining my weekly "plastic art" projects.

ACKNOWLEDGMENTS

I would like to acknowledge my graduate mentor, Lina Ghanbari, for taking me under her wing during my time in the Wiggins research group. Thank you for teaching me mostly everything I know at this point about research, nanomaterials, and many laboratory techniques. This would not have been possible without your patience, kindness, and willingness to help me in all of my endeavors these past two years. Thank you to Dr. Heather Broadhead for helping me in countless endeavors throughout my time at USM and all of your support. I would like to acknowledge Karina Reynolds for conducting the LFA thermal analysis testing and all of your help with the details of this testing. Also, I thank Mr. Michael Blanton for performing the SEM analysis on the thin film samples. I especially want to thank two friends who continuously supported my endeavors and worked alongside me these two years, Zoe Gunter and Zachary Ahmad. I want to thank Dr. Glenn Dale at Pearl River Community College for cultivating my knowledge of chemistry and setting me on the right path towards successfully transferring to USM. Finally, I want to thank my honors thesis research advisor, Dr. Jeffrey Wiggins, for not only allowing me to join the Wiggins group, but also for continuously encouraging my efforts towards a career in polymer science and engineering. Thank you kindly for believing in me and allowing me this opportunity to gain experience as a growing professional.

TABLE OF CONTENTS

LIST OF TABLES

LIST OF ILLUSTRATIONS

LIST OF ABBREVIATIONS

ABS	Acrylonitrile Butadiene Styrene
ATR-FTIR	Attenuated Total Reflectance Fourier Transform Infrared Spectroscopy
FT-IR	Fourier Transform Infrared Spectroscopy
CAD	Computer Aided Design
CFRP	Carbon Fiber Reinforced Polymer Composites
EM	Electromagnetic
EMI	Electromagnetic Interference
GNP	Graphene Nanoparticles
h-BN	Hexagonal Boron Nitride
LFA	Laser Flash Analysis
SEM	Scanning Electron Microscopy
TGA	Thermogravimetric Analysis
TGDDM	Tetraglycidyl 4,4-diaminodiphenylmethane
WRG	Wiggins Research Group
4,4-DDS	4,4-diaminodiphenylsulphone

CHAPTER I: INTRODUCTION

Carbon fiber reinforced polymer composites (CFRP) are a lightweight and high strength metal alternative material used in the aerospace industry; however, they lack the electromagnetic shielding properties necessary for protection against electromagnetic interference (EMI).

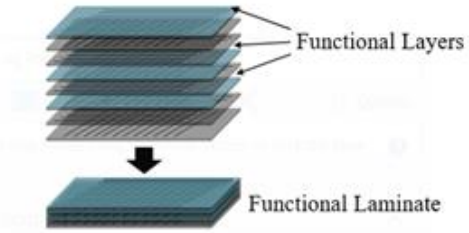

Figure 1. Composite Laminate with EMI/Thermal Diffusion Lamina.

Electromagnentic interference occurs when undesirable radiation causes irreversible damage of essential electronics within a device.[1] Upon interaction of the electromagnetic (EM) wave and an object, electronic interactions can occur based on the degree of electron mobility within the material structure. In electronic devices, this interaction can lead to system malfunction or failure, referred to as EMI.[2] Radiation of varying frequencies can lead to EMI; however, the region of interest for EMI in electronic aircraft systems is the radio to microwave region.[3] EMI can be combatted by employing shielding materials in which electrical and thermal conductivity play a vital role. Shielding can proceed by three different pathways: absorption, reflection, and multiple internal reflections.[4] If radiation is redirected or reflected to an adjacent component, then EMI is not eliminated from the environment and can cause further interference. Therefore, the absorption mechanism is desirable. However, when electromagnetic radiation is converted to thermal energy as it is being absorbed, it can lead to localized heating and cause structural damage.[5]

Accordingly, it is vital for an absorption-dominated shielding material to have both electrical conductivity as well as thermal conductivity.[6] In this regard, metals are

excellent thermal and electrical conductors.[3] Metals such as aluminum, iron, copper, chromium, nickel, brass, and stainless steel can serve as EMI shielding materials, but their bulk densities present difficulty in incorporation into aerospace composites. Furthermore, their high conductivities lead to reflection-dominated shielding, leading to the investigation of lighter alternatives. Nanoparticles such as graphene, carbon nanotubes and metal nanowires are commonly incorporated into polymer matrices as shielding materials and exhibit absorption-dominated shielding.[7] Coatings containing the above materials for shielding are frequently used to combat EMI; however, applying a coating requires undesirable secondary processing.[8] Functional layers containing conductive shielding particles within the composite laminate system as demonstrated in **Fig. 1** eliminate secondary processing such as applying coatings. Multifunctional nanoparticles have previously been employed in aerospace grade matrices to combat EMI; however, little research has been completed about use of multilayer functional materials combining thermally and electrically conductive species. The goal of this research is to investigate how the addition of primarily electrically conductive and thermally conductive (mutually exclusive) nanoparticles in a multifunctional polymer film affects overall shielding efficiency and, ultimately, apply this film as a functional skin onto aerospace grade CFRP. The benefits or disadvantages of combining thermally and electrically conductive materials for the purpose of EMI shielding via the absorption pathway will be investigated. The desired outcome is to determine a successful method for incorporating thermally conductive particles without decreasing electron continuum in the material, which would lead to a decrease in shielding efficiency. To maximize the shielding efficacy of nanomaterials, a percolated network consisting of well dispersed,

exfoliated particles much be achieved; however, one of the challenges of utilizing nanoparticles is re-agglomeration.[9]

Viscosity is a challenge in nanoparticle dispersion as inter-particle forces can lead to agglomeration if the matrix is not sufficiently viscous.[10] Understanding the viscosity of the nanocomposite dispersion over a wide range of temperatures from the uncured, prepolymer state through gelation and, finally, the vitrified, glassy state will yield essential data on manufacturability. Throughout these stages, the particle mobility decreases as molecular weight or network formation persists, as illustrated in **Fig. 2.** In the monomer/oligomer stage, the system has low viscosity, increased flow, and particle mobility. As the system advances to the partially cured stage, a B-staged system that flows with heat is formed, promoting partial particle mobility. Finally, in the fully cured network stage, a vitrified system is formed with no flow and locked particle positions. Optical and scanning electron microscopy will be utilized to observe particle dispersion. Although various matrices are utilized in composites, epoxide/amine-based chemistries are most common in the aerospace industry as of 2020.[11] High performance epoxy amine monomers include tetraglycidyl 4,4-diaminodiphenylmethane (TGDDM), 4,4- diaminodiphenylsulphone (4,4-DDS), and SU-8, an octafunctional cross linking agent with epoxide functionality. Hexagonal boron nitride (h-BN) is a thermally conductive and electrically insulative ceramic material well characterized to exhibit excellent thermal properties.[12] Although h-

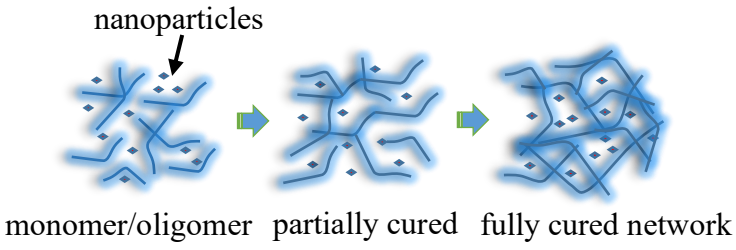

Figure 2. Particle dispersion during matrix advancement.

BN exhibits enhanced thermal conductivity, it is electrically insulative; therefore, incorporation of an electrically conductive nanomaterial is necessary to obtain an interaction with an EM wave. Graphene is a functional material commonly used for applications requiring electrical conductivity.[13] Therefore, hexagonal boron nitride nanoplatelets and graphene nanoplatelets were selected for this work to impart thermal and electrical conductivity. The synthesis of the high-performance aerospace-grade epoxy/amine matrix and the preparation of multifunctional nanocomposite film laminates is presented in the following sections. Multilayer thin film laminates were prepared and characterized via FT-IR to quantify the matrix advancement through various cure states. The dispersion, layer orientation, rheological properties, thermal stability, and thermal conductivity of the multifunctional systems were measured using scanning electron/optical microscopy, parallel plate rheology, thermogravimetric analysis, and Laser Flash Analysis (LFA) thermal diffusivity analysis.

CHAPTER II: EXPERIMENTAL

2.1 Materials

Tetraglycidyl 4,4-diaminodiphenylmethane (TGDDM) was obtained from Royce International (RoyOxy RAR 92L). Micronized 4,4-diaminodiphenylsulphone supplied by Atul (LAPOX® ASH-10 MIC), and SU-8 octafunctional cross linking agent supplied by Hexion (EPON™ Resin SU-8, a.k.a. EPIKOTE™ 157) were utilized. Graphene nanoplates were supplied by Carbon Gates Technologies with a specified diameter of 1-40 μm and a thickness of 1-4 microns. Boron nitride nanoplatelets from U.S. Research Nano Incorporated having an average diameter of 4-6 microns and a thickness of 300 nm were obtained. The monomer structures are depicted in **Fig. 3**. The mechanism of cure and network fragment is depicted in **Figs. 4-6** below.

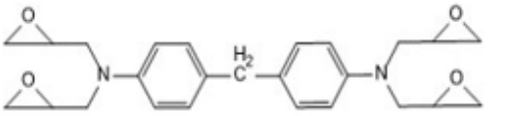

Tetraglycidyl 4,4'-diaminodiphenyl-methane (TGDDM)

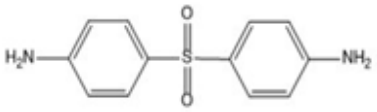

4,4-diaminodiphenyl sulfone (4,4-DDS)

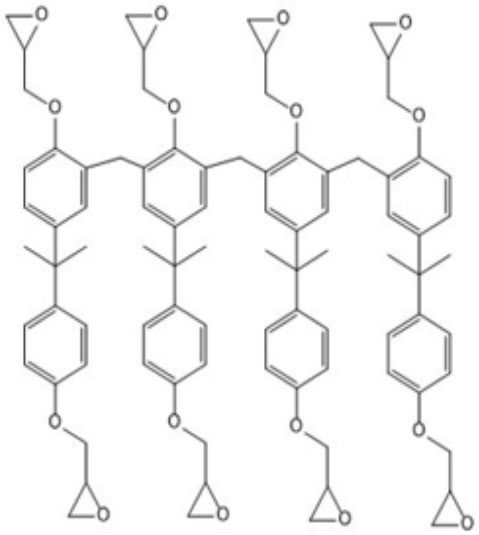

Epon SU-8 (octa-functional epoxide)

Figure 3. Monomer structures.

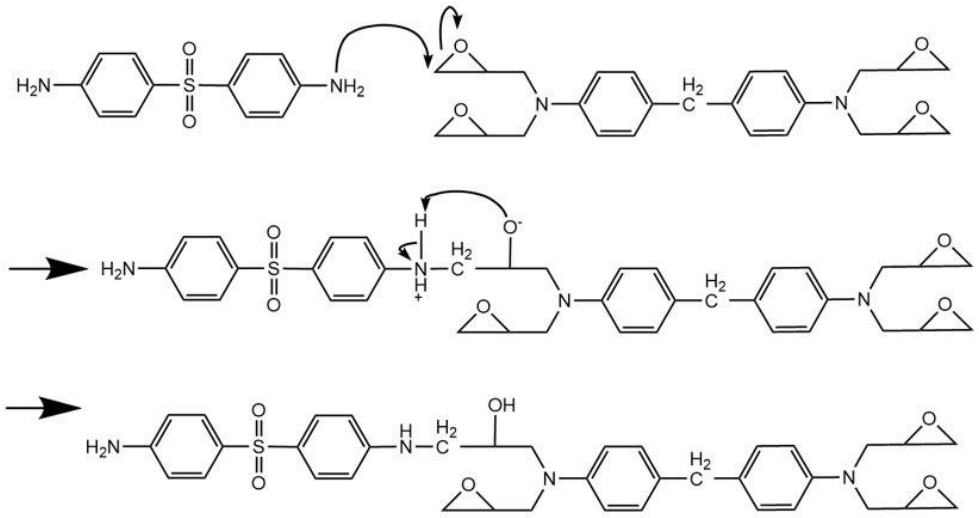

Figure 4. Nucleophilic addition mechanism.

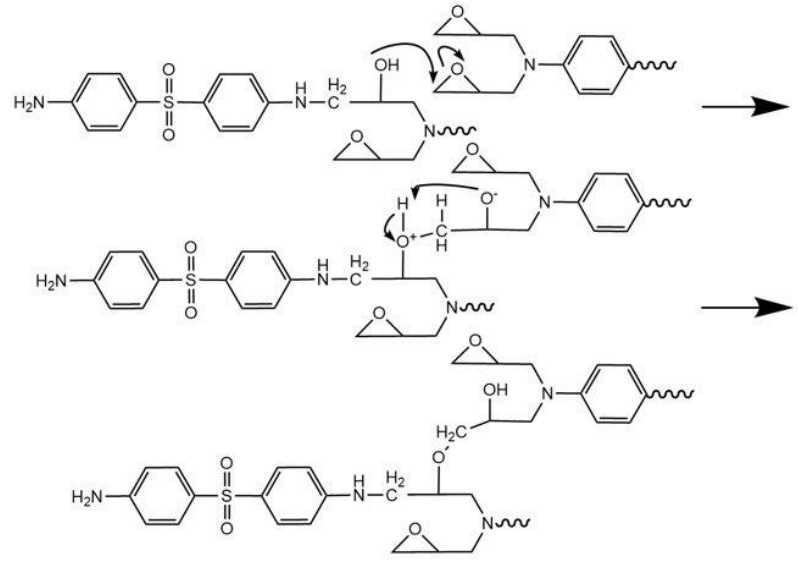

Figure 5. Etherification mechanism.

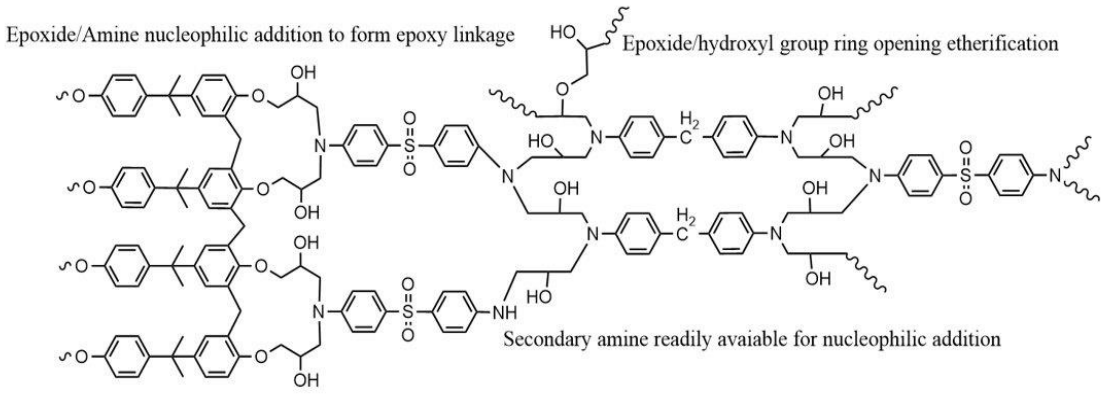

Figure 6. Fragment of cured network.

2.2 Preparation of Polymer Matrix and Dispersions

Epoxy polymer matrix was prepared using TGDDM, 4,4-DDS, and SU-8 octafunctional cross linking agent. Stored, frozen TGDDM monomer was warmed to room temperature before heating to 80°C for 30 minutes to obtain a pourable viscosity. Next, the appropriate amount of matrix was weighed in a 100 mL beaker. The matrix was placed in a chemical hood on a magnetic stir/heat plate at a temperature of 115°C with an external thermocouple in contact with the glass apparatus and submerged approximately 1.27 cm in the polymer matrix. A magnetic stir bar was placed in the prepolymer, with a stir rate set at 50 rpm. Next, solid crystal-like SU-8 was weighed and added incrementally to the matrix, solubilizing after 10 minutes. The appropriate amount of solid powder 4,4-DDS was weighed and slowly added to the solution in small increments, clarifying in approximately 15 minutes after all material was added. After clarity was observed, the sample was transferred into a capped FlackTeK speed mixer cup, weighed to obtain the total mass, and quenched via storage in a freezer. This process was repeated three times

to synthesize three batches of neat epoxy/amine prepolymer matrix. After the frozen prepolymer matrix was warmed to room temperature, the samples were placed in an oven at 80°C for 30 minutes once more to obtain a viscous liquid. Graphene nanoparticles and hexagonal boron nitride nanoplatelets were added to separate neat matrix materials at 1 wt.%, without any stirring. Following the addition of nanoplatelets, the FlackTek cups containing the samples were placed in a lab-scale FlackTek speed mixer for two 30 second cycles at a speed of 300 rpm, after which samples resembled homogenous dispersions. Samples were then frozen and stored until further use.

2.3 Preparation of Mold and Multifunctional Films

To obtain thin film samples of appropriate geometries and desired thickness for laboratory-scale analysis, a silicon mold was cast from a 3D-printed depression mold. A depression mold was designed to produce 22 mm, square shaped samples of 0.1, 0.2, and 0.4-mm thickness, respectively. The mold design was developed in SolidWorks CAD software. A dimensioned blueprint is depicted in **Fig. 7, panel A**. The depression mold was 3D-printed from Ultimaker Black ABS filament. The mold was subsequently polished utilizing sandpaper to remove excess material and/or undesired texturing from the mold surface. Next, a 2-part silicon mixture was poured into the plastic mold and degassed in a vacuum oven to remove excess air and/or moisture. Once all air was removed, the mold was cured overnight at ambient temperature, and the cured material was removed from the base mold to realize a solid silicon mold with a release finish. The mold was then post-cured using the prescribed intended film cure protocol. The final mold is depicted below in **Fig. 7, panel B**.

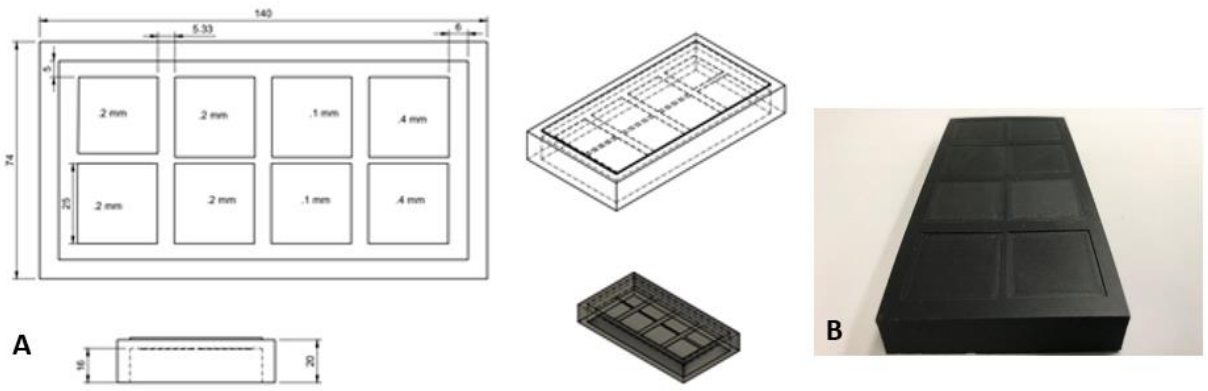

Figure 7. Mold schematic and final mold: A) 2D drawing of depression mold (mm), B) Silicon mold for film preparation.

The appropriate amount of material required to fill each mold well was calculated using the bulk density to find the necessary volume of each sample. Utilizing the determined conditions from rheology experiments included in the following sections and prior research within the WRG a cure cycle was decided. The mold wells were filled with neat, h-BN, and graphene nanoparticle GNP samples. Initially, samples were heated at 80°C for 18 hours to advance the epoxide-amine reaction to a "workable" consistency. Samples were then layered before curing for an additional 6 hours at 80°C. The samples were cured for 1 hour at 180°C with a 2°C/min thermal ramp from 40-180°C, followed by a 2-hour post-cure incubation at 220°C to form vitrified, glassy films. A total of four sample types were prepared: 1) two alternating 0.2 mm layers of GNP and h-BN, 2) one 0.4 mm neat polymer matrix as control, 3) one 0.4 mm GNP layer, and 4) one 0.4 mm h-BN layer. A process schematic is depicted in **Fig. 8**.

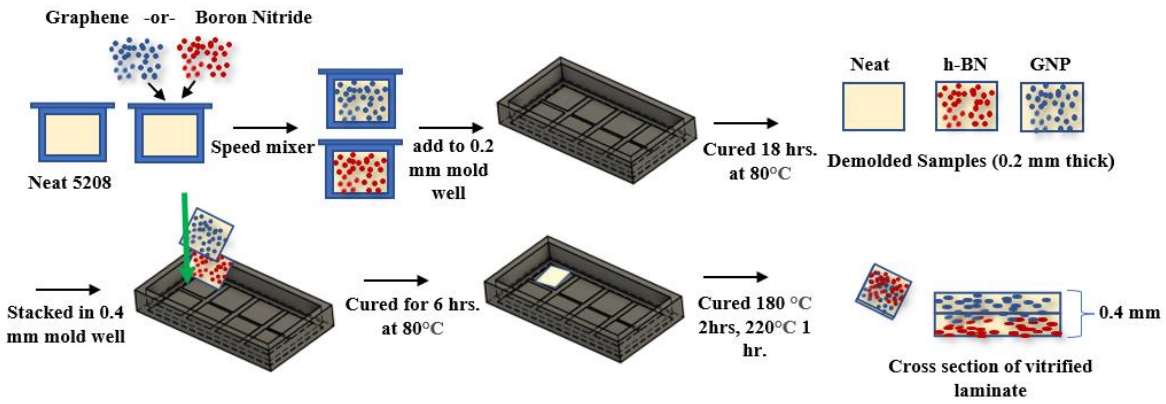

Figure 8. Processing schematic for laminates.

CHAPTER III: CHARACTERIZATION

3.1 Optical Microscopy

An Olympus GX51 optical microscope with a magnification of 20x was utilized to acquire images of the pre-cured materials and the 18-hour cured materials. The samples were prepared by applying pressure to material placed between a glass slide and a coverslip. No additional heat was applied to maintain particle orientation in-situ to initial processing conditions to avoid manipulating particile dispersion by heat.

Additionally, a Zeiss Smart Zoom 5 optical microscope was utilized to acquire images of the post-cured bilayer films. Samples were prepared by fracturing to expose cross sections of bilayer films for analysis of layer orientation.

3.2 Multifrequency Oscillatory Rheology

Standard oscillatory multi-wave tests of uncured neat and loaded materials were acquired utilizing a TA Instruments Ares G2 parallel plate rheometer at frequencies of 5, 10, 20, 30, 40, 50, and 80 rad/s with a 2°C thermal ramp from 40 to 220°C. Aluminum disposable parallel plates with a diameter of 25 mm were utilized. A plate gap of 1 mm was targeted. Plates were pre-conditioned and brought to temperature before a sample was added. Samples were prepared by acquiring small shards of neat, GNP- and h-BN-loaded samples by shattering frozen samples for placement on heated plates. The experiment was monitored until the viscosity was observed to significantly increase, indicating gelation, at which point the acquisition was stopped.

3.3 Scanning Electron Microscopy.

A Zeiss Sigma Variable Prime scanning electron microscope with a VP mode vacuum level of 10^{-9} Torr in atmospheric nitrogen was utilized to acquire images, identify

discrete layer makeup, and characterize initial nano materials. In addition to the precursor materials, Scanning Electron Microscopy (SEM) was acquired for the bilayer film cross sections to qualify discrete layer formation. All images were captured using an accelerating voltage of 20 KeV.

3.4 Fourier Transform infrared (FT-IR) spectroscopy.

A PerkinElmer Frontier ATR FT-IR spectrometer was utilized to acquire 16 scans per sample with a resolution of 4. FT-IR was performed on the neat, h-BN, and GNP samples throughout the uncured, 18 hour, and 24 hour cure profile states.

3.5 Thermogravimetric Analysis (TGA)

A TGA Q50 instrument was utilized to measure the mass loss as a function of temperature for the control samples as well as bilayer samples. Samples of 10-12 mg, fractured from the post-cured films, were utilized for each analysis. A thermal ramp from ambient to 600°C with a ramp rate of 10°C per minute was performed.

3.6 Laser Diffusivity Analysis (LFA)

An LFA 4600 flash laser thermal diffusivity analyzer with a pulse width of 0.6 ms and a 250 eV accelerating electron voltage was utilized to calculate specific heat, thermal conductivity, and thermal diffusivity of neat, h-BN, GNP, and multilayer samples. A graphite reference sample was utilized. Samples were trimmed to disks with 9 mm diameters and treated with a graphitic coating before analysis.

CHAPTER IV: RESULTS

4. 1 Film Preparation

The material consistency was investigated at each preparation step to predict workability and tack for film layering. Several pilot trials were conducted to investigate material consistency and workability at room temperature. As seen by the following images, the consistency of the films reached sufficient tackiness and workability after cure for 18 hours at 80°C to be manually demolded and assembled. After being demolded and stacked in two lamina sequences in the 0.4 mm mold wells, the mold was returned to the oven for an additional 6-hour cure at 80°C for a total of 24 hours at 80°C. After the 24-hour cure, samples were placed in a programmable cure oven with a thermal ramp from 40-180°C at 2°C per minute with a 2-hour isothermal cure at 180°C. Then, an additional thermal ramp from 180 to 220°C at 2°C per minute was implemented with a final isothermal post-cure for 1 hour at 220°C. After the post cure, samples were demolded and prepared for various characterization techniques. The final samples were glassy and vitrified. The material at each stage of the cure profile is depicted in **Fig. 9**. The films progressed from highly viscous liquids to solid, glassy layers.

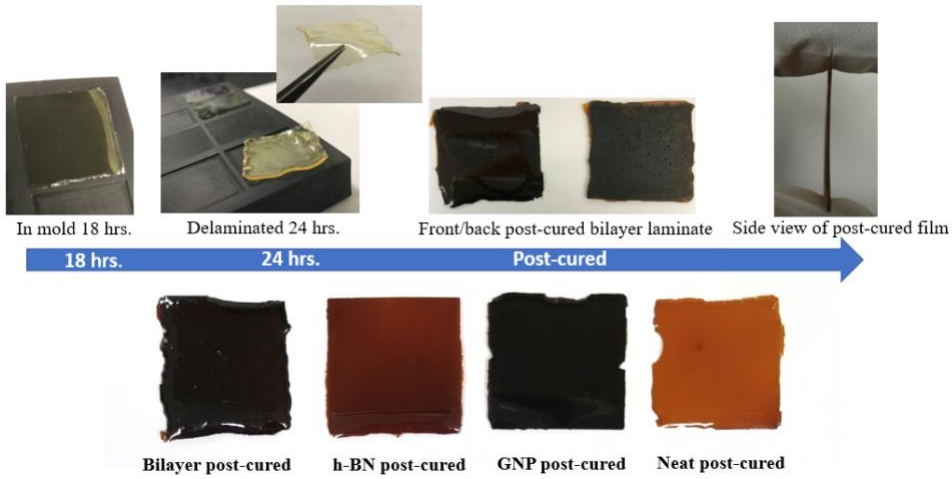

Figure 9. Samples throughout cure protocol and final vitrified films: Initially, films are visous liquids placed in mold well. After various cyles of time/temperatures, solid, glassy layers are formed (fully cured films).

4. 2 Optical Microscopy

The resulting images of the prepolymer material and 18-hour cured samples are depicted in **Fig. 10**. Images of the post-cured bilayer films are included in **Fig. 11**. Initial microscopy of the prepolymer materials depicted in **Fig. 10** showed evidence of particle migration from the pre-cure-18 hour cure states. Large areas of dark agglomerates can be seen in the 18-hour samples in panels E-H of **Fig.10**. However, these areas of dark agglomerates diminish to relatively small areas in panels A-D, indicating the particles have migrated and dispersed more regularly throughout the matrix after heat and force from processing was applied. The final vitrified multilayer films depicted in **Fig. 11**, panels B and D exhibited formation of distinct layers visible upon examining the final cross-sections. The h-BN nanoparticles are a fine, white powder; whereas, the GNP materials are dark grey/black. The lighter layer is postulated to be the h-BN layer, while the darker layer is the GNP layer. Granulation is indicative of nanoparticles.

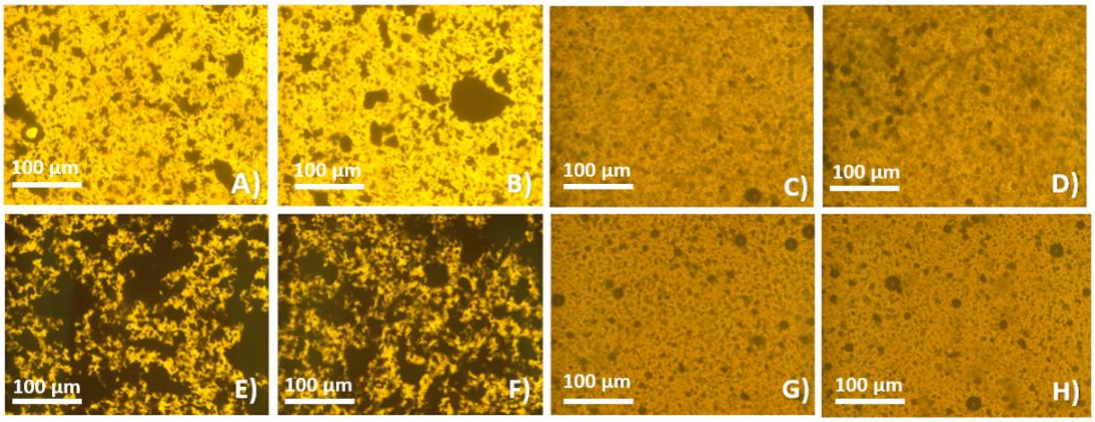

Figure 10. Microscopy of dispersions pre-post heat/processing stages. A) and B) GNP 18 hour hold; C) and D) h-BN 18 hour hold; E) and F) GNP pre-cure; G) and H) h-BN pre-cure. All images were taken at 20x magnification.

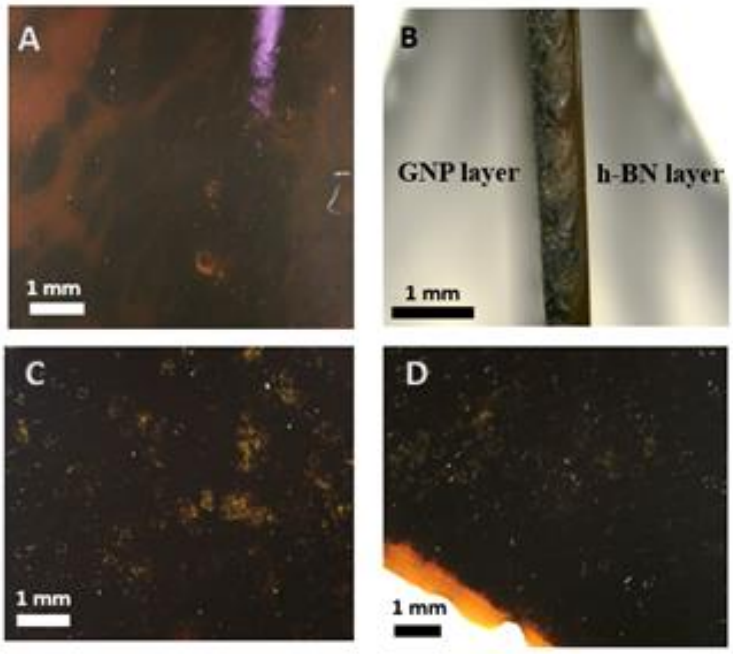

Figure 11. Microscopy images of post-cured bilayer film samples. A) h-BN top side of film 50x, B) Cross section of bilayer film 70x, C) GNP bottom side of film 50x, D) Distinct edge cross section from bottom angled view 70x.

4. 3 Scanning Electron Microscopy (SEM)

The respective SEM images of the raw nanomaterials are depicted in **Figs. 12 and 13**. Images of the two-layer films are depicted in **Fig. 14**. The images of the nanomaterials indicated average dimensions concurrent with the reported specifications from the supplier; however, large agglomerations and a broad range of platelet sizes were discovered through SEM analysis. Final imaging of the vitrified bilayer films and single layer films depicted uniform film thicknesses and no evidence of porosity, indicating successful consolidation of uniform films. Additionally, no topographical evidence of interlaminar separation in the bilayer films was visible in **Fig. 14**, panel A. It is therefore postulated that the polymer matrix layers achieved co-cured properties without undesirable spacing or delamination between layers. This is suggested visually through SEM in **Fig.13**, as no evidence of void space between layers in the film cross section is indicated (continuous film).

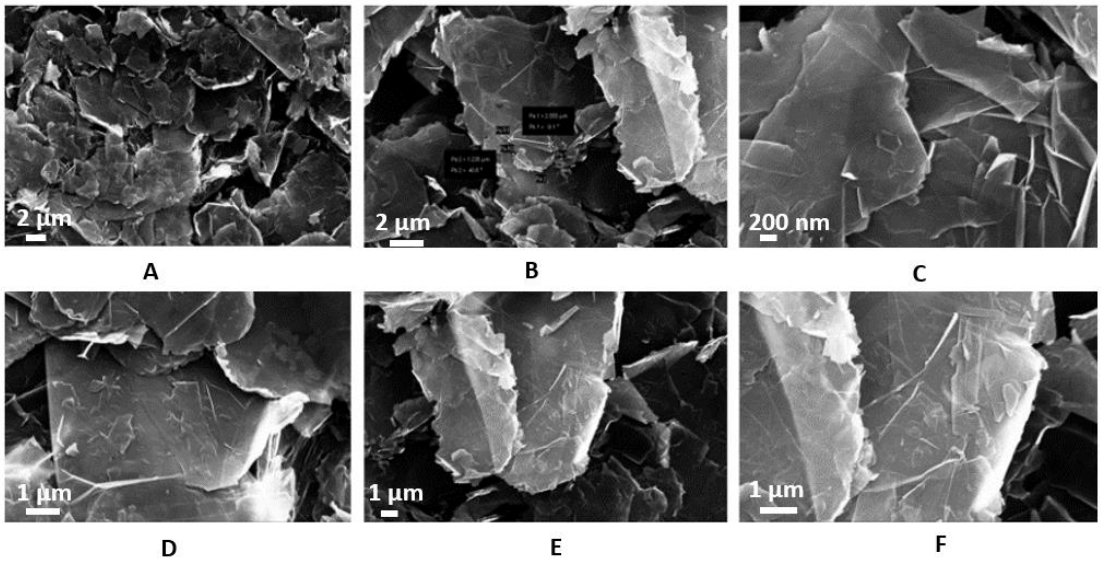

Figure 12. SEM images of GNP: A) 2,000x, B) 5,000x, C) 20,000x, D) 10,000x, E) 5,000x, and F) 10,000x.

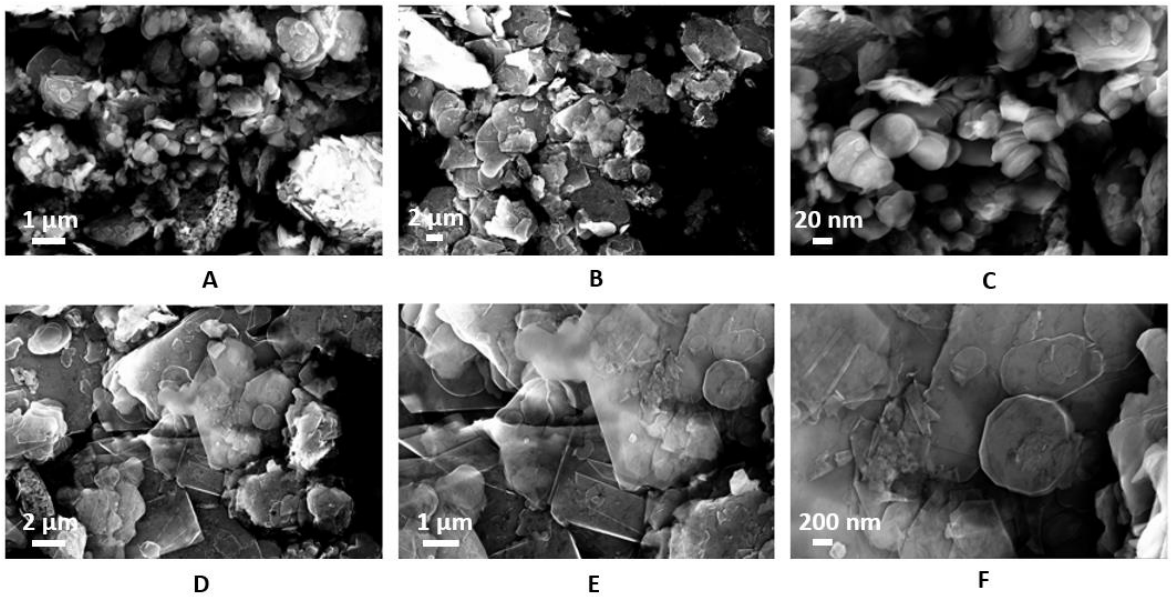

Figure 13. SEM images of h-BN: A) 10,000x, B) 2,000x, C) 25,000x, D) 5,000x, E) 10,000x, and F) 20,000x.

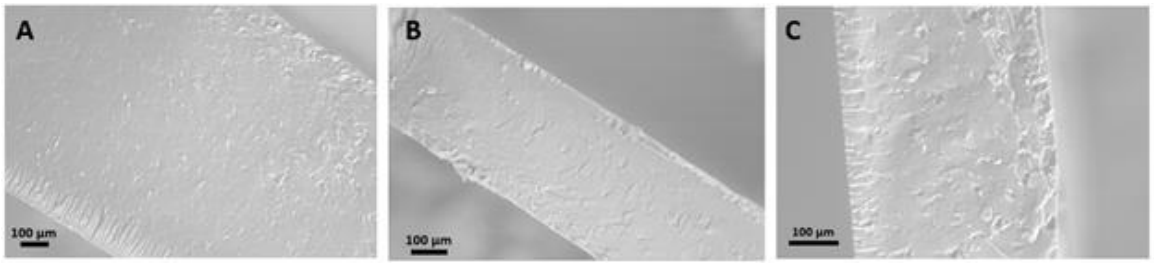

Figure 14. SEM of film cross sections. A) Bilayer film cross section at 80x magnification, B) h-BN film cross section at 100x, and C) GNP film cross section at 150x.

4. 4 Rheology

Prior work in the WRG showed that particle agglomeration persisted at 1 Pa.s in the case of carbon nanotubes.[14] Therefore, the viscosity at 80°C was verified to be above 1 Pa.s for each sample to avoid agglomeration during processing. Within this same work, a proposed cure profile was determined to maintain appropriate viscosity and minimize particle agglomeration (isothermal hold at 80°C for 18 hours, then cure at 180°C for 2 hours followed by post cure at 220°C for 1 hour). This method was initially followed;

however, particle migration was visible in initial trial cure cycles. Accordingly, the 80°C cure protocol hold was increased to 24 hours. This method provided more particle stability, and no evidence of migration was observed. **Figs. 15 and 16** depict the rheological testing results. Rheological testing resulted in similar values of viscosity and point of gelation without observing drastic modifications in viscosity at 80°C or the temperature at the point of gelation. Table 1 contains a summary of the results.

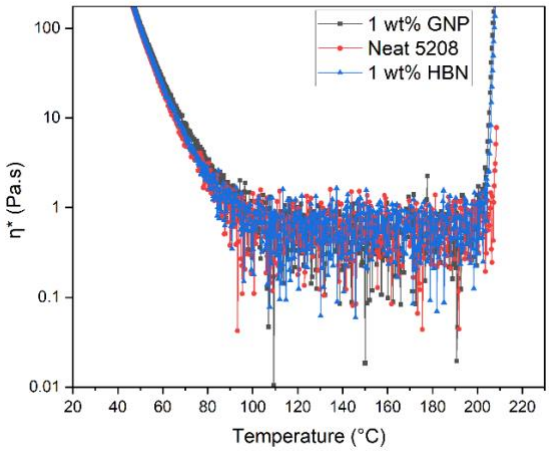

Figure 15. Complex viscosity summary curve of h-BN, GNP, and neat samples at 30 rad/sec.

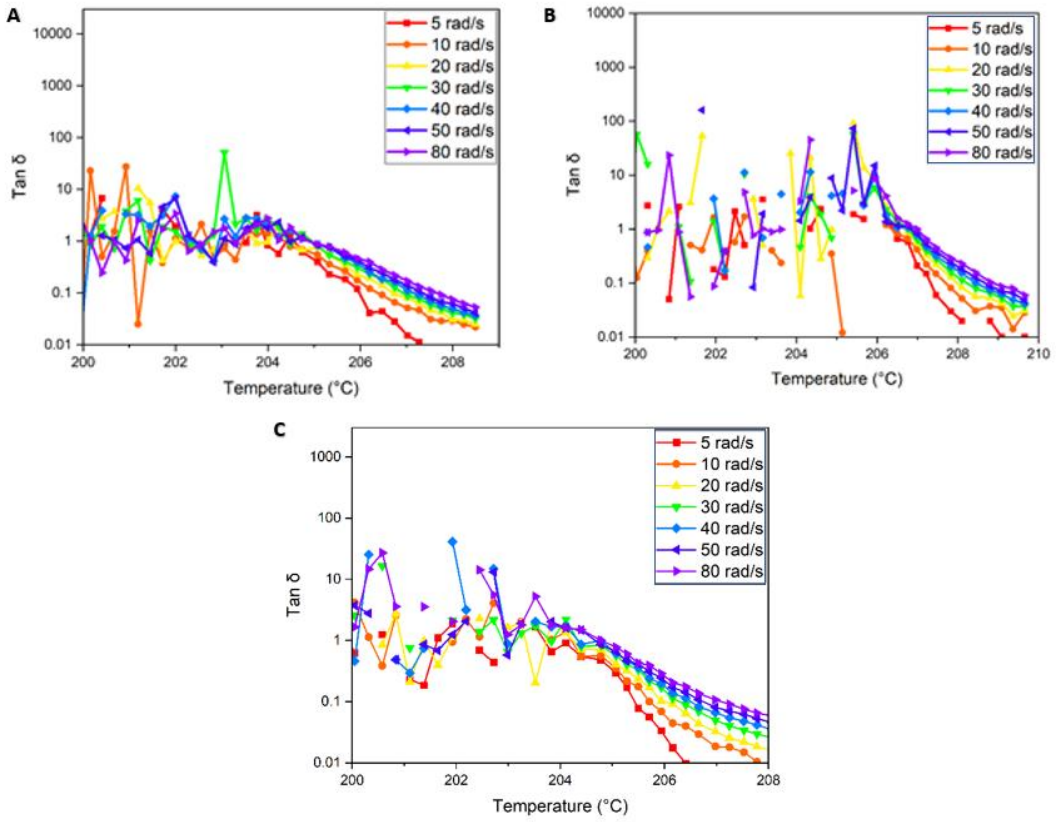

Figure 16. Multifrequency sweep Tan δ intersection summary: A) GNP sample, B) neat sample, C) h-BN sample.

Table 1. Summary of rheology results.

Parameter	Neat	GNP	h-BN
Point of gelation (°C)	206.5	204.48	204.11
Viscosity at 80°C (Pa·s)	2.72	3.35	2.00

4.5 Thermogravimetric Analysis

The resulting 5 wt.% loss and char yield is depicted in Table 2. **Figure 17** contains a summary curve of the weight percent loss of each sample as a function of temperature. The h-BN sample resulted in a slightly reduced char yield and higher T5% (temperature at 5% initial mass loss) compared to the other samples. Although this

difference could be attributed to greater thermal stability imparted by the h-BN material, the values could indeed be statistically the same upon multiple successive analyses and the resulting standard deviation. Prior research investigating the effects of h-BN inclusion in composite matrices found that slight improvements in char yield and degradation temperature are imparted by incorporation of h-BN. However, this phenomenon is more distinct at higher loading levels.[15]

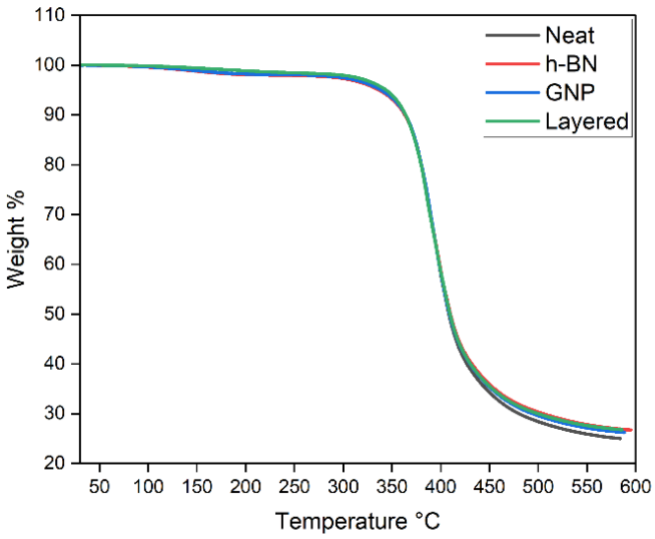

Figure 17. TGA weight % loss as a function of temperature overlay.

Table 2. TGA results.

Result	Bilayer	Neat	h-BN control	GNP control
T5% (°C)	338.69	337.65	344.08	336.53
Char yield (%)	26.12	26.73	24.84	26.64

4.6 Fourier Transform Infrared Spectroscopy

The resulting FT-IR spectra from the uncured-post-cured states are included in **Fig. 18**. An equation was utilized to calculate the percent cure throughout the stages of time/heat cycles. The equation utilized to calculate the degree of conversion by calculating the change in area ratios of a reactive (epoxide) and unreactive (aromatic) moiety is depicted in Equation 1. The following peak assignments were utilized: C-C aromatic peak (1509-1515 cm^{-1}), C-O epoxide peak (905-907 cm-1). The aromatic peak area was utilized as the internal reference in Eq. 1. The results in Table 3 indicated similar cure progressions, with the uncured samples collected immediately upon liquid/solid clarification in the prepolymer preparation considered to be the zero percent cured point in Eq. 1. The post-cured results indicated similar cure progression with values of 80.97%, 76.64%, and 82.68 % cure for the neat, h-BN, and GNP samples, respectively. The cure progression of the h-BN sample was the least advanced, indicating that the inclusion of h-BN could influence cure progression. However, it is postulated based on prior work that particle agglomeration could lead to decreased cure progression in polymer matrices.[16]

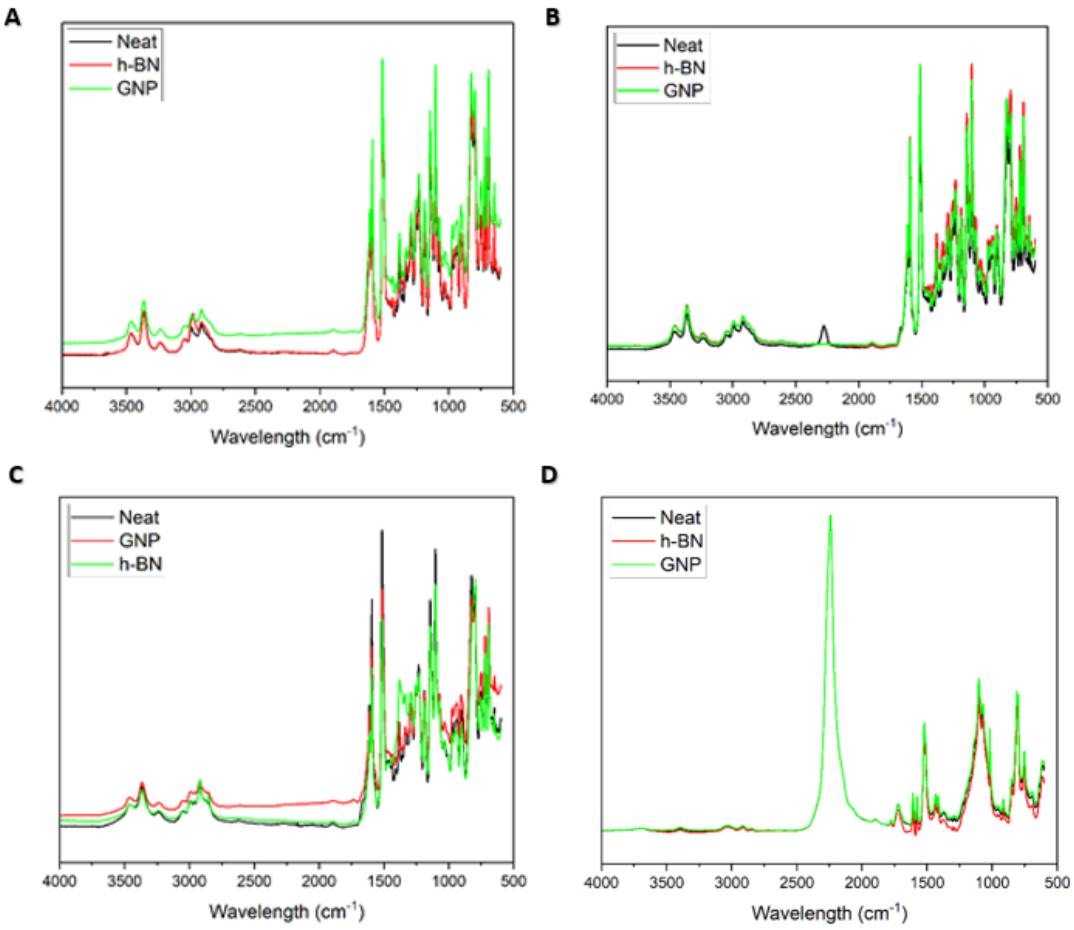

Figure 18. FT-IR spectra: A) Uncured samples, B) 18 hour cure sample, C) 24 hour cure sample, D) Post-cure samples.

$$Degree\ of\ Conversion = \frac{\left(\frac{A_{Epoxide}}{A_{Internal\ Standard}}\right)_0 - \left(\frac{A_{Epoxide}}{A_{Internal\ Standard}}\right)_t}{\left(\frac{A_{Epoxide}}{A_{Internal\ Standard}}\right)_0} * 100\% \quad (1)$$

Table 3. FT-IR results.

Sample	Uncured % cure	18 hour % cure	24 hour % cure	Post-cured % cure
Neat	0	18.38	25.59	80.97
h-BN	0	17.72	26.02	76.64
GNP	0	18.85	22.11	82.68

4. 7 Laser Flash Diffusivity Analysis

Resulting measurements of through-plane thermal conductivity and thermal diffusivity are depicted in Table 4. Because the laser beam is applied from one direction, two film orientation sequences were investigated: h-BN layer closest to laser beam source and GNP layer closest to laser beam source. The thermal diffusivity as well as the thermal conductivity increased from the neat to the h-BN, GNP, and the layered samples. Although the GNP samples exhibited the highest conductivity among the monolayer samples, both orientations of the layered samples superseded conductivity and diffusivity of all samples. The layered samples proved to increase thermal conductivity exponentially relative to the neat samples. The multilayer sample with the GNP face upwards (in the sample chamber, the bilayer film was placed with the GNP layer on the top) resulted in the highest thermal diffusivity as well as thermal conductivity aside from the reference.

$$Degree\ of\ Conversion = \frac{\left(\frac{A_{Epoxide}}{A_{Internal\ Standard}}\right)_0 - \left(\frac{A_{Epoxide}}{A_{Internal\ Standard}}\right)_t}{\left(\frac{A_{Epoxide}}{A_{Internal\ Standard}}\right)_0} * 100\%$$

Table 4. Laser flash analysis thermal results.

Sample	Diffusivity (mm2/s)	Conductivity (W/(m*K)
Neat	0.277	0.275
h-BN	3.85	3.819
GNP	108.866	107.777
Multi-Layer (h-BN Up)	308.268	302.411
Multi-Layer (GNP Up)	556.115	545.549
Graphite Reference	1231.128	2129.852

CHAPTER IV: CONCLUSION

The data collected confirmed that inclusion of multilayer thermally and electrically conductive species improve thermal conductivity significantly compared to neat and single layer control films. Multilayer sequencing of h-BN- and GNP-modified polymer matrices improved both thermal conductivity and thermal diffusivity values. Additionally, conductivity and diffusivity values were manipulated by alternating the sequences of the same materials relative to an applied energy source. Furthermore, the inclusion of the nanoparticles utilized resulted in miniscule alteration of polymer properties such as point of gelation, cure progression, degradation temperature, and char yield. However, a slight improvement in char yield and degradation temperature for h-BN-containing samples was observed. The proposed cure protocol and processing method resulted in workable films with the ability to be sequenced to form vitrified bilayer films, with discrete layers confirmed through microscopy analysis.

The results of this endeavor were then expected based upon the initial hypothesis that inclusion of both thermally and electrically conductive species could increase thermal conductivity of a multifunctional epoxy system. These results signify that discrete layers of thermally and electically conductive layers can be maintained in a multifunctional laminate system utilizing the prescribed time/temperature processing steps described in this work to improve thermal properties of the polymer matrix. This work indicates that the inclusion of these multifunctional nanoparticles can be achieved without altering crucial processing parameters of the polymer matrix such as time/temperature to gelation, degredation temperature, char yield, cure progression, and viscosity. Therefore, the process utilized in this work offers a successful alternative for

forming multilayer, multifunctional nanocomposite films in future scalable applications using alternate processing with similar thermal profiles.

The Wiggins Research Group at The University of Southern Mississippi aims to design aerospace composite materials that fit the needs of the current aerospace industry. This includes the need for materials capable of EMI shielding using aerospace approved materials to guarantee rapid implementation of the new technology. This current research could be extended by incorporating such films into aerospace grade composite laminates and by scaling up the manufacturing of particle/matrix blends to produce high quality monolayer and bilayer films. Subsequently, the electrical conductivity of these multifunctional systems should be defined (measured and quantified via an acceptable scientific instrument which is currently unavailable within the facilities at USM) to determine if the pathway for electrical conductivity is maintained in systems containing both thermally and electrically conductive systems as fabricated in this work.

REFERENCES

1) Liang, J.; Wang, Y.; Huang, Y.; Ma, Y.; Liu, Z.; Cai, J.; Zhang, C.; Gao, H.; Chen, Y. Electromagnetic Interference Shielding of Graphene/Epoxy Composites. *Carbon* **2009**, *47*, pp. 922–925
2) Al-Saleh, M. H.; Sundararaj, U. X-Band EMI Shielding Mechanisms and Shielding Effectiveness of High Structure Carbon Black/Polypropylene Composites. *J. Phys. D: Appl. Phys.* **2013**, *46* (3), 035304.
3) Geetha, S.; Satheesh Kumar, K.K.; Rao, C.R.; Vijayan, M.; Trivedi, D.C. EMI Shielding: Methods and Materials—A Review. *J. App. Poly. Sci.* **2009**, *112*, pp. 2073-2086.
4) Sankaran, S.; Deshmukh, K.; Ahamed, M. B.; Pasha, S. K. K. Recent Advances in Electromagnetic Interference Shielding Properties of Metal and Carbon Filler Reinforced Flexible Polymer Composites: A Review. *Composites Part A: Applied Science and Manufacturing* **2018**, *114*, 49–71.
5) Banerjee, P.; Bhattacharjee, Y.; Bose, S. Lightweight Epoxy-Based Composites for EMI Shielding Applications. *Journal of Electronic Materials* **2020**, *49* (3), 1702–1720.
6) Al-Saleh, M. H.; Sundararaj, U. Electromagnetic Interference Shielding Mechanisms of CNT/Polymer Composites. *Carbon* **2009**, *47* (7), 1738–1746.
7) Ganguly, S.; Bhawal, P.; Ravindren, R.; Das, N.C. Polymer Nanocomposites for Electromagnetic Interference Shielding: A Review. *J. Nanosci. Nanotech.* **2018**, *18*, pp. 7641-7669.
8) Russ, M.; Rahatekar, S.S.; Koziol, K.; Farmer, B.; Peng, H.X. *Comp. Sci. Tech*. **2013**, *81*, pp. 42–47.
9) Li, X.; Long, Y.; Ma, L.; Li, J.; Yin, J.; Guo, W. Coating Performance of Hexagonal Boron Nitride and Graphene Layers. *2D Materials* **2021**, *8* (3), 034002.
10) Electromagnetic interference shielding behavior of hybrid carbon nanotube/exfoliated graphite nanoplatelet coated glass fiber composites. Materials Science and Engineering: B. 248. 114403.
11) Gnidakouong, Joel & Kim, Joo-Hyung & Kim, Hansang & Park, Young-Bin. (2019).
12) Banerjee, P.; Bhattacharjee, Y.; Bose, S. Lightweight Epoxy-Based Composites for EMI Shielding Applications. *J. Electron. Mater*. **2020**, *49*, pp. 1702–1720
13) Lee, E.-S.; Kang, J.-G.; Kang, M.-K.; Kim, K.-H.; Park, S.-T.; Kim, Y. S.; Kim, I.; Kim, S.-D.; Bae, J.-Y. High Thermal Conductivity of Boron Nitride Filled Epoxy Composites Prepared by Tin Solder Nanoparticle Decoration. *Composites Part B: Engineering* **2021**, *225*, 109264.
14) Li, C.-B.; Li, Y.-J.; Zhao, Q.; Luo, Y.; Yang, G.-Y.; Hu, Y.; Jiang, J.-J. Electromagnetic Interference Shielding of Graphene Aerogel with Layered Microstructure Fabricated via Mechanical Compression. *ACS Appl. Mater. Interfaces* **2020**, *12* (27), 30686–30694.
15) Mathew, H. Multifunctional Nanocomposites Prepared via Continuous High Shear Reactor. PhD, The University of Southern Mississippi, Hattiesburg, MS, May 2020.

16) Isarn, I.; Ramis, X.; Ferrando, F.; Serra, A. Thermoconductive Thermosetting Composites Based on Boron Nitride Fillers and Thiol-Epoxy Matrices. *Polymers* **2018**, *10*, p. 277.
17) Zhan, Y.; Lago, E.; Santillo, C.; Del Río Castillo, A. E.; Hao, S.; Buonocore, G. G.; Chen, Z.; Xia, H.; Lavorgna, M.; Bonaccorso, F. An Anisotropic Layer-by-Layer Carbon Nanotube/Boron Nitride/Rubber Composite and Its Application in Electromagnetic Shielding. *Nanoscale* **2020**, *12*, pp. 7782–7791.